Supporting Information

Camilloni et al. 10.1073/pnas.1404220111

SI Text

NMR Measurements. ***Chemical shifts in the free state.*** Recombinant ^{13}C,^{15}N-labeled cyclophilin A was purified as described previously (1). Briefly, ^{13}C,^{15}N-labeled cyclophilin A was concentrated to ∼1.0 mM protein in 50 mM Na_2HPO_4 (pH 6.5), 2 mM DTT with 10% D_2O, which was the NMR solution buffer. All spectra were collected on either a Varian 600 MHz or 800 MHz spectrometer at 10 °C and at 25 °C, which included a standard Biopack HNCACB and CBCAcoNH. Data were processed using NMRPipe (2) and analyzed using CcpNmr software (3).

Chemical shifts and intermolecular NOEs in the bound state. To obtain NMR measurements in the bound state of cyclophilin A with the GSFGPDLRAGD peptide substrate, two samples were produced. The first sample contained 0.5 mM ^{13}C,^{15}N-labeled cyclophilin A and 4 mM of unlabeled peptide, and the second sample contained 0.5 mM ^{13}C,^{15}N-labeled peptide with 4 mM of unlabeled cyclophilin A. This two-sample strategy was used because of the relatively weak binding constant between cyclophilin A and the peptide substrate, which makes it impossible to approach saturation for both the enzyme and the peptide. Instead, a 1:8 ratio allows ∼97% binding, such that the chemical shifts report on the bound form. This strategy also reduces peak overlap. The buffer described above for the free enzyme was used. Because the *cis*-to-*trans* and *trans*-to-*cis* substrate isomerization rates are 1,040/s and 1,640/s, respectively (4), catalysis is within the fast exchange regime. Thus, chemical shifts during catalysis obtained for each of the two samples described above provide values averaged over the *cis*-bound and *trans*-bound states. At these concentrations the enzyme and peptide are about 97% bound. C13/N15-edited/filtered intermolecular NOESY experiments, Biopack sequence gCNfilnoesyChsqcSA, were collected using these two samples, and the resulting NOEs were used for the calculations.

Residual dipolar couplings in the free state. Commercially available bicelle mixtures were found to interact specifically with the hydrophobic active site of cyclophilin A as monitored through ^{15}N-heteronuclear single-quantum coherence (HSQC) spectroscopy experiments. As previously described, specific mixtures offer optimal alignment at different temperatures. Thus, C12E5/hexanol mixtures were produced for amide residual dipolar couplings (RDCs) collected at 25 °C, whereas C8E5/octanol mixtures were produced for amide RDCs collected at both 10 °C and 0 °C. For example, 30 μL of polyethylene glycol was added to the NMR solution buffer, and alcohols were added at microliter increments; during these additions the monodeuterated water splitting was used to monitor alignment of these mixtures. Finally, 60 μL of 1.1 mM ^{15}N-labeled cyclophilin A was added to 240 μL of the aligned mixtures, and standard in-phase/anti-phase experiments were collected on a Varian 900 MHz at the Rocky Mountain Regional 900 MHz NMR Facility at the three temperatures described above.

Molecular Dynamics Simulations. ***General setup.*** All the simulations in the present work were performed using GROMACS (5). The system was simulated using the Amber99SB*-ILDN force field (6, 7) in explicit TIP3P water (8). A time step of 2 fs was used together with LINCS constraints (9). van der Waals interactions were cut off at 1.2 nm, and long-range electrostatic interactions were treated with the Particle Mesh Ewald method (10). The canonical ensemble was enforced by keeping the volume fixed and by thermosetting the system with the Bussi thermostat (11). The starting conformation for the free state was taken from the NMR structure of Protein Data Bank (PDB) ID code 1OCA (12); the structures of PDB ID codes 1M9C and 1M9Y were used for the *cis*-bound and *trans*-bound states, respectively (13). The structures were protonated and solvated with 5,102 TIP3P water molecules in a dodecahedron box with a volume of 178 nm^3. First, the energy of the system was minimized, and then the temperature was increased to 300 K in two separate steps. In the first step a 50-ps simulation was performed by keeping the heavy atoms of the protein fixed; then a second 200-ps simulation was performed without any restraint. The density of the system was relaxed by a 200-ps run using the Berendsen barostat (14).

Replica-averaged ensemble. The starting structures for the two replicas of the system were selected as the final structure from two simulations, each 1 ns long. Experimental chemical shifts for the free and bound state were measured as described in the *NMR* section above and were applied as a restraint over the two replicas of the system as shown previously for ribonuclease A (15). CamShift (16) was used to back-calculate the chemical shifts from both replicas at each time step. In the bound case, the NOEs between the protein and the substrate were applied on the two replicas as average restraints (17, 18).

The force constant for the chemical shifts restraints was set to 5.2 kJ/mol, and the force constant for the NOEs was set to 250 $kJ{\cdot}mol^{-1}{\cdot}nm^{-2}$ with a bottom flat potential that is zero between 0.3 and 0.5 nm. In term of energy per atom, the contribution of the chemical shifts restraint was less than 0.4 kJ/mol (<3% of the total), and the contribution of the NOEs was less than 0.02 kJ/mol (<1% of the total). Each replica has been evolved through a series of annealing cycles between 300 K and 450 K (100 ps at 300 K, 100 ps during which the temperature increased linearly up to 450 K, 100 ps of constant-temperature molecular dynamics at 450 K, and 300 ps during which the temperature decreased linearly to 300 K). Only structures from the 300-K segment of the simulation are taken into account for analysis. Each replica has been evolved for a total nominal time of 100 ns. The final ensembles comprise all the 300-K structures sampled by both replicas.

The averaged chemical shift restraints were added to GROMACS by using PLUMED (19) and Almost. The NOEs were added using the module already provided within GROMACS.

Quantum Mechanical Calculations. All the quantum mechanical (QM) calculations were done using the Gaussian 03 suite of programs (20).

Investigation of electric field effects on the ω–ψ potential energy surface of a proline model. The starting calculations aimed to reveal the presence of electrostatic field effects on the energy barrier of ω rotation at the substrate proline site. A bicapped L-proline was used as a model to study the influence of electrostatic fields (Fig. S4). The acetylic (*Ace*) and *N*-methyl amino (*Nme*) groups were added at the L-proline imino and carboxyl termini, respectively. The resulting structure (*N*-acetyl-L-prolyl-*N*-methylamide, Ace-Pro-Nme) is the simplest model for studying the properties of a proline residue while maintaining relatively correct electronic states of the terminal atoms that, in a full-scale polypeptide structure, participate in peptide bonding with the adjacent amino acid residues.

Hybrid-density functional theory (DFT) (21) was used with the Becke three-parameter exchange functional and the Lee, Yang, and Parr correlation functional (22–24) (B3LYP) for all QM calculations in this work.

The geometry of the model was constructed manually using mixed Cartesian and internal coordinates to maintain a fixed direction for the molecule-associated coordinate system over the course of conformational changes in the molecule but retaining the ability to relax the structure fully when a complete geometry optimization was needed. The origin of the coordinate system is set at the N atom of proline, with the *x* axis always pointing along the N–C bond and the *z* axis orthogonal to the plane of the proline ring as represented in Fig. S2*B*. The choice of the axis directions also accounted for the predicted most influential directions for the uniform electric fields. The *y* direction is along the (H)–N bond and is parallel to the C=O bonds of the peptide bond that defines the ω rotation, with (H) being a carbon atom in the case of proline imino acid. The *z* axis points in the direction of the formation of a nonconventional hydrogen-bond between the proline nitrogen and the guanidinium moiety of arginine or histidine from an enzyme-binding site. This hydrogen bond represents a widely accepted mechanism for the action of the proline isomerization enzymes (25). In many cases hydrogen bonding can be regarded as a type of electric field effect (26); hence the further generalization of the H-bonding as electric field effects seems to be a reasonable explanation for the actions of cyclophilins. Overall, the *x* and *z* directions selected for the further application of a uniform electric field should be most influential in changing the energetic characteristics of the ω rotation.

The initial structure of Ace-Pro-Nme was fully geometry optimized with a split-valence 6–31G(d,p) basis set (27). This step was followed by a complete scan of the ψ and ω space, spanning the range of −180° to 180° for both angles with angle steps of 15°. For each ψ/ω configuration, the geometry was optimized with preset ψ and ω angles in nine different conditions, overall completing 5,625 (25 × 25 × 9) hybrid-DFT calculations. The nine conditions include eight calculations with uniform electric fields of −50, −20, 0, 20, and 50 MV/cm (the minus signs indicate the reverse direction) applied along the *x* and *z* directions and a single calculation without any external field application. The complete set of results is presented in Fig. S4, where the energy of the Ace-Pro-Nme system is plotted against the ω and ψ angles under the above conditions. The energy is presented in kilojoules per mole, referenced by the lowest energy conformation observed in each of the computed landscapes. The difference map between the corresponding electric field condition and the normal, gas-phase (no field) condition clearly highlights the regions in the ψ/ω space where the electric field stabilizes (blue) or destabilizes (red) the system (Fig. S4).

As can be inferred from the potential energy surface plots, the electric field acting along both the *x* and *z* directions has a substantial impact on the pathway of the ω-rotation reaction. It is clear that the electric fields along the *–x, x, –z*, and *z* directions facilitate ω rotations by decreasing the relative barrier for the transitions at the 0/+, +/(−,+), 0/+ and +/− regions correspondingly. In *a*/*b* notation, *a* indicates the region of the ψ dihedral angle (around 0, + for positive ψ, and − for negative ψ), and *b* denotes the same for ω (Fig. S4). Hence, the fine interplay of electrostatic fields acting along different directions is capable of modulating the pathway for the proline *cis–trans* transitions.

Natural bond orbital analysis of Ace-Pro-Nme. To clarify whether the effect of the electric field on the ω-rotation barrier is the result of substantial changes in the electronic structure at the proline site, we performed a natural bond orbital (NBO) (28, 29) analysis of Ace-Pro-Nme, paying attention to the bonding orbital along the N–C bond that defines the ω rotation. In particular, if the influence of the external electric field were mediated through abrupt changes in electronic structure, one would expect a decrease in the population of the N–C bonding orbital components and/or a decrease in the contributions from the natural atomic orbitals in *p* components and increase in these contributions in *s* components. With such changes, the N–C bond can become more of an *s* type and less of a *p* type, thus making the rotation along the bond relatively more feasible.

However, the results show only slight differences in such populations upon the application of the electric field. For instance, the selected model transition structure with ω = 90° and ψ = −10°, for which a substantial reduction of the potential energy is observed while applying −50-MV/cm field along the *z* axis (Fig. S4*B*), changes the N–C binding natural molecular orbital from [0.7903($sp^{2.39}$) + 0.6128($sp^{2.22}$)] to [0.7911($sp^{2.45}$) + 0.6117($sp^{2.29}$)], as expressed in the established notation system for the NBO analysis and omitting negligible *d* contributions. The first term in the addition comes from N atoms, and the second term from C atoms. The polarization coefficients, if squared, show the percentage of the NBO on each N-based or C-based hybrid. Shown below is the state of the N–C bonding NBO with and without a −50 MV/cm uniform electric field, with the whole system expressed in percentages and the *sp* hybrids broken down into separate *s* and *p* contributions:

Electrostatic field = 0 MV/cm

NBO occupancy = 1.98605

Orbital energy = −0.75419 Hartree

N (62.45% contribution, of which 29.45% is *s* character and 70.50% is *p* character)

C (37.55% contribution, of which 31.02% is *s* character and 68.84% is *p* character)

Electrostatic field = − 50 MV/cm along the *z* axis

NBO occupancy = 1.98519

Orbital energy = −0.74989 Hartree

N (62.58% contribution, of which 28.97% is *s* character and 70.97% is p character)

C (37.42% contribution, of which 30.34% is *s* character and 69.52% is *p* character)

Hence, the electrostatic field affected the overall electron occupancy of the N–C bonding NBO only slightly, increasing (slightly destabilizing) the orbital energy by ∼11.3 kJ/mol and slightly increasing the *p* character of the contributing natural atomic orbitals. Similar negligible effects are observed in similar calculations using the *cis* (ω = 0° and ψ = −10°) and *trans* (ω = 180° and ψ = −10°) structures of the proline model instead of the transition-state structure.

Therefore, the observed stabilization of the transition structure is the result of the overall electrostatic interaction of the substrate molecule with the external electric fields rather than specific modulation of the electronic structure that would affect the N–C bond of the ω rotation.

QM studies of the electric fields in the active site of cyclophilin A. The calculations for the proline residue model detailed above clearly demonstrate that electric fields with values within the range typical for biomolecules (30) can be influential in defining ω-rotation energy barriers. Here we also verify that the fields of such magnitude are acting in cyclophilin A active site.

For the QM calculations on the cyclophilin A active site, 114 structures from each of the obtained *cis* and *trans* ensembles were geometry optimized with an Amber99SB*-ILDN force field (6, 7). The maximum allowed force acting on any atom was set at 100 kJ/nm. An active region is defined for cyclophilin A via an *n*-layered integrated molecular orbital plus molecular mechanics method (ONIOM) (31) routine in Gaussian 03. The region is determined first by counting all the atoms within a 7.5-Å radius from the nitrogen atom of the substrate proline. Next, the fragments from the residues that were halved by this definition were extended to complete the residues or, in the case of large

residues, to extend the moieties toward a chemically sensible partition. The latter step has set the distance of the most distant (from proline N) counted atoms at around 12 Å. The resulting QM region included 250 atoms from Arg-55, Ile-57, Phe-60, Met-61, Gln-63, Met-100, Ala-101, Asn-102, Ala-103, Phe-113, Trp-121, Leu-122, Lys-125, and His-126 (Fig. S3).

In this way, ONIOM calculations are done for all of the 228 structures from *cis* and *trans* ensembles. Single-point calculations were done with B3LYP/6–31G(d,p) level of theory for the system inside the QM region. Dummy atoms replaced the substrate atoms, so that only the electrostatic contribution from cyclophilin A was counted, and the place markers for the substrate atoms were retained. Electrostatic effect embedding was not allowed; hence the electric fields in the cyclophilin A active site reflect only the QM component from the defined region. Then, electric field values were retrieved for the position of the substrate N atom of the proline residue and then were projected into the x and z coordinates of the proline N-fixed coordinate system.

All the calculations described here were repeated for the equivalent set of structures from *cis* and *trans* ensembles with the R55A mutation.

1. Schlegel J, et al. (2009) Solution characterization of the extracellular region of CD147 and its interaction with its enzyme ligand cyclophilin A. *J Mol Biol* 391(3):518–535.
2. Delaglio F, et al. (1995) NMRPipe: A multidimensional spectral processing system based on UNIX pipes. *J Biomol NMR* 6(3):277–293.
3. Vranken WF, et al. (2005) The CCPN data model for NMR spectroscopy: Development of a software pipeline. *Proteins* 59(4):687–696.
4. Eisenmesser EZ, et al. (2005) Intrinsic dynamics of an enzyme underlies catalysis. *Nature* 438(7064):117–121.
5. Hess B, Kutzner C, van der Spoel D, Lindahl E (2008) Gromacs 4: Algorithms for highly efficient, load-balanced, and scalable molecular simulation. *J Chem Theory Comput* 4(3):435–447.
6. Best RB, Hummer G (2009) Optimized molecular dynamics force fields applied to the helix-coil transition of polypeptides. *J Phys Chem B* 113(26):9004–9015.
7. Lindorff-Larsen K, et al. (2010) Improved side-chain torsion potentials for the Amber ff99SB protein force field. *Proteins* 78(8):1950–1958.
8. Jorgensen WL (1981) Quantum and statistical mechanical studies of liquids. 10. Transferable intermolecular potential functions for water, alcohols, and ethers - application to liquid water. *J Am Chem Soc* 103:335–340.
9. Hess B (2008) P-lincs: A parallel linear constraint solver for molecular simulation. *J Chem Theory Comput* 4:116–122.
10. Essmann U, et al. (1995) A smooth particle mesh Ewald method. *J Chem Phys* 103: 8577–8593.
11. Bussi G, Donadio D, Parrinello M (2007) Canonical sampling through velocity rescaling. *J Chem Phys* 126(1):014101.
12. Ottiger M, Zerbe O, Güntert P, Wüthrich K (1997) The NMR solution conformation of unligated human cyclophilin A. *J Mol Biol* 272(1):64–81.
13. Howard BR, Vajdos FF, Li S, Sundquist WI, Hill CP (2003) Structural insights into the catalytic mechanism of cyclophilin A. *Nat Struct Biol* 10(6):475–481.
14. Berendsen HJC, Postma JPM, van Gunsteren WF, Dinola A, Haak JR (1984) Molecular-dynamics with coupling to an external bath. *J Chem Phys* 81:3684–3690.
15. Camilloni C, Robustelli P, De Simone A, Cavalli A, Vendruscolo M (2012) Characterization of the conformational equilibrium between the two major substates of RNase A using NMR chemical shifts. *J Am Chem Soc* 134(9):3968–3971.
16. Kohlhoff KJ, Robustelli P, Cavalli A, Salvatella X, Vendruscolo M (2009) Fast and accurate predictions of protein NMR chemical shifts from interatomic distances. *J Am Chem Soc* 131(39):13894–13895.
17. Lindorff-Larsen K, Best RB, Depristo MA, Dobson CM, Vendruscolo M (2005) Simultaneous determination of protein structure and dynamics. *Nature* 433(7022): 128–132.
18. Richter B, Gsponer J, Várnai P, Salvatella X, Vendruscolo M (2007) The MUMO (minimal under-restraining minimal over-restraining) method for the determination of native state ensembles of proteins. *J Biomol NMR* 37(2):117–135.
19. Bonomi M, et al. (2009) PLUMED: A portable plugin for free-energy calculations with molecular dynamics. *Comput Phys Commun* 180:1961–1972.
20. Frisch MJ, et al. (2004) *Gaussian 03, revision c.02* (Gaussian, Inc, Wallingford, CT).
21. Kohn W, Sham LJ (1965) Self-consistent equations including exchange and correlation effects. *Phys Rev* 140:1133–1138.
22. Lee C, Yang W, Parr RG (1988) Development of the Colle-Salvetti correlation-energy formula into a functional of the electron density. *Phys Rev B Condens Matter* 37(2): 785–789.
23. Becke AD (1993) Density-functional thermochemistry. 3. The role of exact exchange. *J Chem Phys* 98:5648–5652.
24. Miehlich B, Savin A, Stoll H, Preuss H (1989) Results obtained with the correlation-energy density functionals of Becke and Lee, Yang and Parr. *Chem Phys Lett* 157: 200–206.
25. Schroeder OE, et al. (2006) Theoretical and experimental investigation of the energetics of cis-trans proline isomerization in peptide models. *J Phys Chem A* 110(20):6522–6530.
26. Sahakyan AB, Shahkhatuni AG, Shahkhatuni AA, Panosyan HA (2008) Electric field effects on one-bond indirect spin-spin coupling constants and possible biomolecular perspectives. *J Phys Chem A* 112(16):3576–3586.
27. Krishnan R, Binkley JS, Seeger R, Pople JA (1980) Self-consistent molecular-orbital methods. 20. Basis set for correlated wave-functions. *J Chem Phys* 72:650–654.
28. Foster JP, Weinhold F (1980) Natural hybrid orbitals. *J Am Chem Soc* 102:7211–7218.
29. Reed AE, Weinhold F (1983) Natural bond orbital analysis of near-Hartree-Fock water dimer. *J Chem Phys* 78:4066–4073.
30. Suydam IT, Snow CD, Pande VS, Boxer SG (2006) Electric fields at the active site of an enzyme: Direct comparison of experiment with theory. *Science* 313(5784):200–204.
31. Vreven T, Morokuma K (2000) On the application of the IMOMO (integrated molecular orbital plus molecular orbital) method. *J Comput Chem* 21:1419–1432.
32. Fraser JS, et al. (2009) Hidden alternative structures of proline isomerase essential for catalysis. *Nature* 462(7273):669–673.

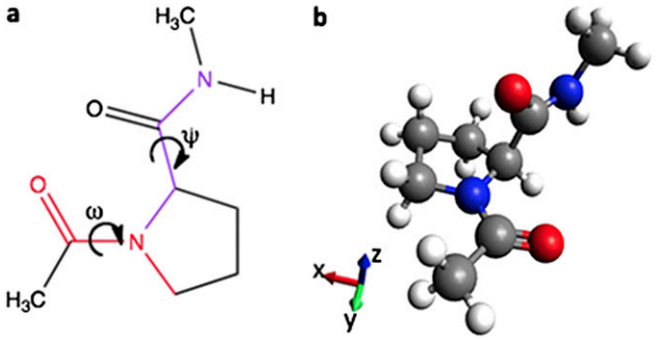

Fig. S1. Molecular model used to obtain the energy profiles of proline conformational transitions at different electric field values and directions. (*A*) The ω and ψ dihedral angles, further used as potential energy-surface coordinates, are highlighted. (*B*) An example of the geometry is shown with the directions of the coordinate system that is attached to the N atom of proline.

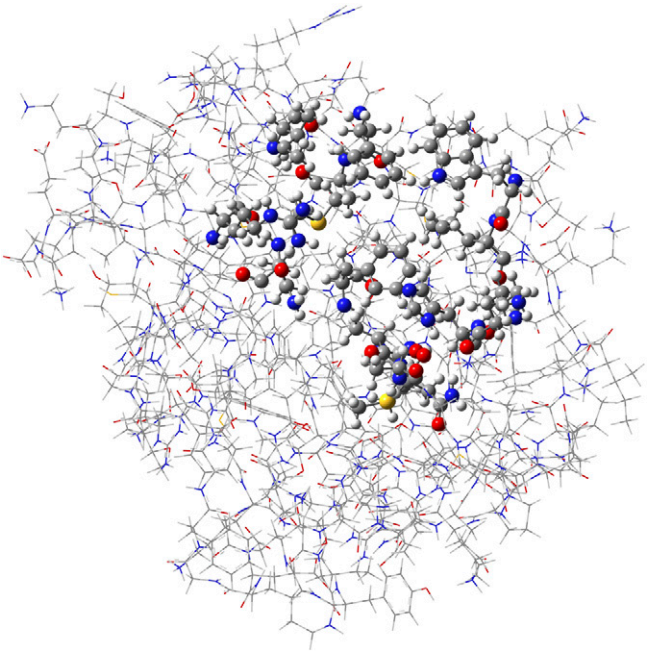

Fig. S2. Structure of cyclophilin A showing the QM region around the active substrate-binding site highlighted in ball-and-stick representation.

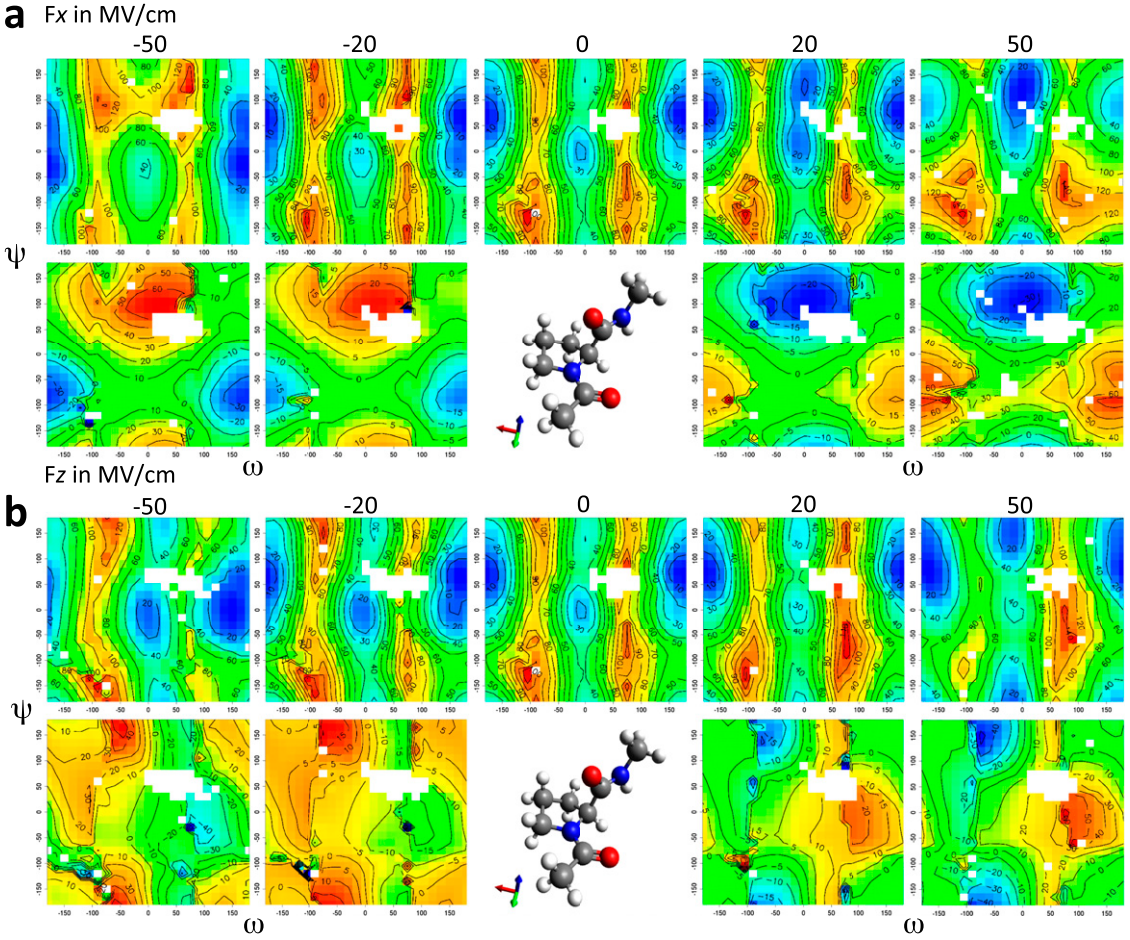

Fig. S3. Potential energy surfaces for Ace-Pro-Nme across ψ/ω space without and with uniform electric field acting along the *x* (*A*) and *z* (*B*) directions. The color scheme (from blue to red) and the isocontour lines depict the energy in kilojoules per mole. The lower rows in *A* and *B* show difference maps calculated with respect to the model system in the absence of an electric field.

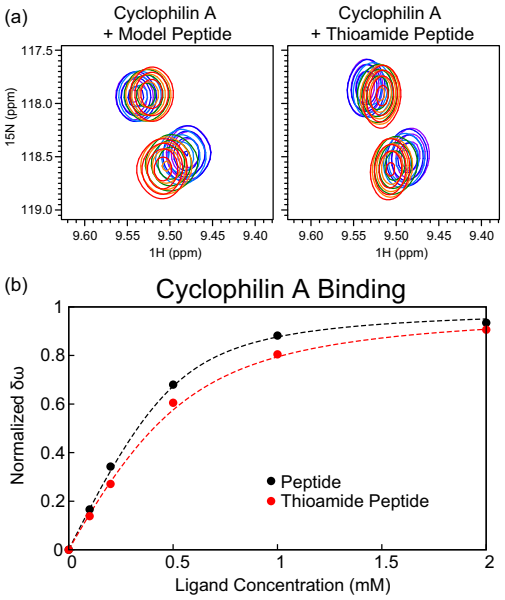

Fig. S4. Binding of the thioamide-substituted peptide. (*A*) HSQC spectra of 0.5 mM ^{15}N CypA alone (red) or with addition of 0.1 mM (orange), 0.2 mM (green), 0.5 mM (light blue), 1 mM (dark blue), and 2 mM (violet) model peptide (*Left*) or thioamide-substituted peptide (*Right*). (*B*) Normalized binding isotherm for a single residue in CypA during titration of the model peptide (black) and modified peptide (red). Dotted lines represent best-fit curves using the dissociation constant determined by simultaneous fitting to multiple peaks for each titration. The dissociation constants for the model and thioamide-substituted peptide are 76 ± 6 μM and 156 ± 16 μM, respectively.

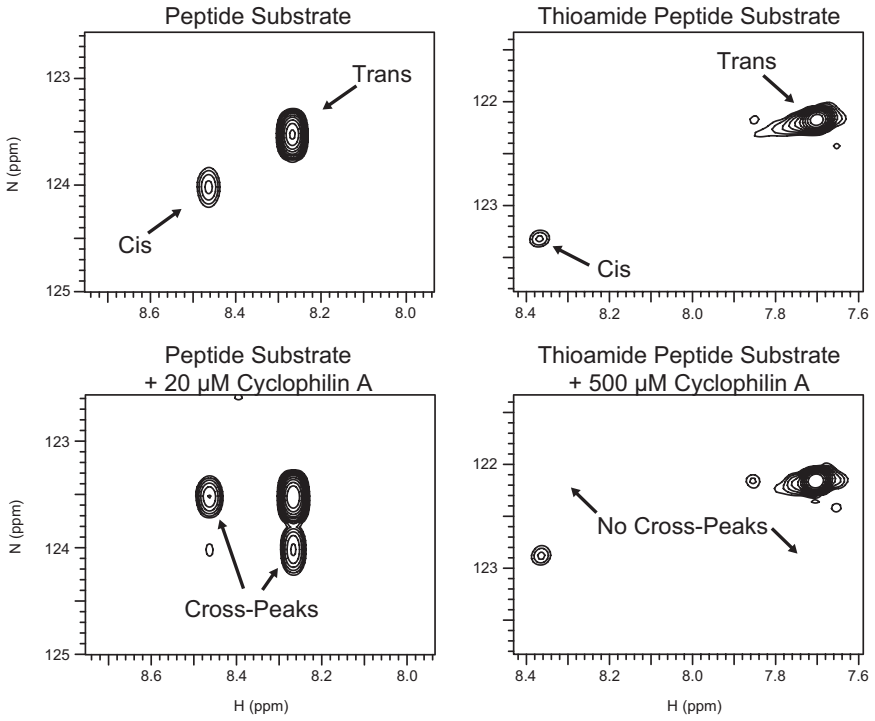

Fig. S5. Comparison of the ZZ-exchange spectra of the model peptide substrate and its thioamide variant. The spectra of the peptides alone and with cyclophilin A (20 μM added to the normal peptide, 500 μM added to the thioamide peptide variant) are shown. Although there are no cross-peaks in the thioamide peptide variant, even with 500 μM cyclophilin A, the *cis* peak is shifted significantly, consistent with the observation that cyclophilin A binds to the *cis* conformation. These results indicate that the thioamide substitution almost completely stops the turnover of the substrate.

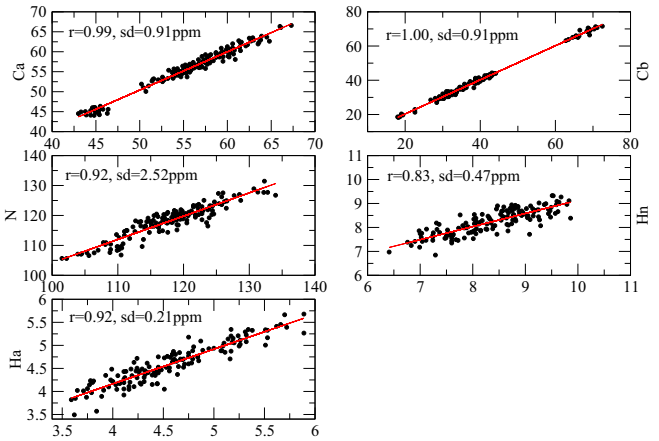

Fig. S6. Comparison of the experimental and calculated chemical shifts for the free-state ensemble of cyclophilin A. *r*, correlation coefficient; sd, SE.

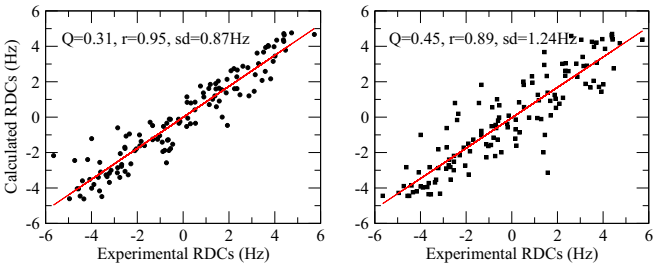

Fig. S7. Comparison of the experimental and calculated RDCs. (*Left*) Free ensemble of cyclophilin A. (*Right*) The structure of PDB ID 1OCA. Q, quality factor; r, correlation coefficient; sd, SE.

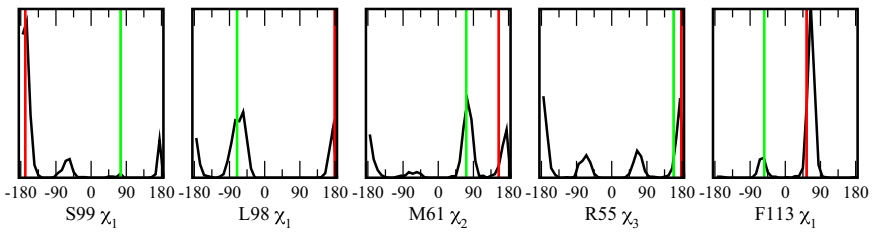

Fig. S8. Comparison of dihedral angles in the free conformations determined by Fraser et al. (32) and in the present study. The black line represents the free-state ensembles of cyclophilin A; the red and green bars represent the major and minor population, respectively, as determined by Fraser et al. (32).

Table S1. Distances (in nanometers) for the hydrogen atom pairs restrained with NOE-derived distances

Atom pairs	*cis* subensemble	*trans* subensemble	Whole ensemble	Experimental range
73Hg–1Ha	0.43	0.53	0.46	0.2–0.6
73Hg–2Ha	0.37	0.31	0.33	0.2–0.6
73Hg–2Hb	0.42	0.44	0.43	0.2–0.6
73Hg–3Hd	0.51	0.50	0.51	0.2–0.6
73Hg–3He	0.49	0.52	0.51	0.2–0.6
100He–3Hd	0.40	**0.84**	0.44	0.2–0.6
100He–3He	0.36	**0.77**	0.40	0.2–0.6
102Ha–3Hd	0.41	0.30	0.33	0.2–0.6
102Ha–3He	0.44	0.35	0.38	0.2–0.6
102Hb–3Hd	**0.67**	0.57	0.60	0.2–0.6
102Hb–3He	**0.70**	0.57	0.61	0.2–0.6
107Hb–3Hd	0.45	0.50	0.47	0.2–0.6
107Hb–3He	0.30	0.31	0.30	0.2–0.6
107Hg–3Hd	**0.66**	**0.72**	**0.68**	0.2–0.6
107Hg–3He	0.55	0.56	0.55	0.2–0.6
108Ha–3Hd	**0.70**	0.56	0.60	0.2–0.6
108Ha–3He	0.58	0.42	0.46	0.2–0.6
122Hd–6Ha	0.59	**0.65**	0.61	0.2–0.6
122Hd–6Hb	0.42	**0.61**	0.46	0.2–0.6
148Hg–7Hd	**0.66**	0.48	0.52	0.2–0.6
148Hd–7Hd	0.60	0.52	0.55	0.2–0.6
57Hd–7Hd	0.41	0.45	0.43	0.2–0.6
57Hg–7Hd	0.41	0.36	0.38	0.2–0.6
60Ha–7Hd	0.58	0.55	0.56	0.2–0.6
60Hb–7Hd	0.40	0.36	0.23	0.2–0.6
61He–7Hd	0.53	**0.77**	0.59	0.2–0.6
119Hg–7Hd	**0.71**	**0.69**	**0.70**	0.2–0.6

The columns show the averages for the *cis*-bound and *trans*-bound subensembles and for the whole bound ensemble. Values in bold are outside the experimental bounds.

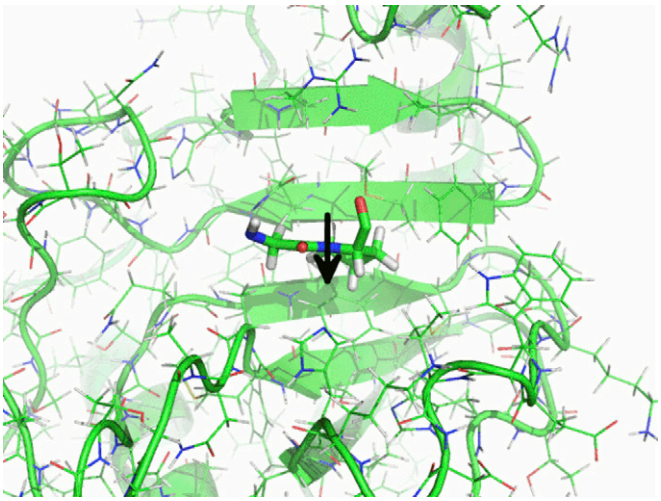

Movie S1. Illustration of the electrostatic handle mechanism. (*Left*) The electrostatic field (black arrow) in the catalytic site of cyclophilin A acts on the electric dipole associated with the carbonyl group of the glycine residue preceding the proline residue in the peptide substrate, thus favoring its rotation. (*Right*)The energy barrier for the rotation is shown as a function of the ω (*x*-axis) and ψ (*y*-axis) backbone dihedral angles.

Movie S1